Contoured Bode Plot-Based Robust Controller Design and Analysis of a Three-Input Integrated Bidirectional C-DC Converter for Microgrid Application

KOTTALA PADMA, M. MANOGNA, B. AMARENDRA REDDY
Department of Electrical Engineering,
Andhra University College of Engineering,
Visakhapatnam, Andhra Pradesh,
INDIA

Abstract: - Many power electronic applications, such as locomotives and Hybrid Electric Vehicles (HEVs), are moving towards a Multi-Input Multi-Output (MIMO) integrated DC-DC converter for its reliability and flexibility. This work proposes a Three-Input Integrated Bidirectional DC-DC (TIIBD) Converter to combine a Photovoltaic (PV) panel, Fuel Cell (FC) stack, and battery for grid-connected Hybrid Energy Microgrids (HEMs), enabling bidirectional power flow and energy storage. The TIIBD converter is modeled using state-space analysis, yielding a Transfer Function Matrix (TFM). PV and FC are optimized for maximum power via the P&O MPPT algorithm and CRCBP-based PI control. A 3-level Neutral Point Clamped (NPC) Inverter is used for power management between the grid and the TIIBD converter. The controllers for the three inputs are designed, and the steady-state performance of the converter with an AC load of 10KW for Microgrid (MG) application in different operating conditions is analysed and verified in MATLAB/Simulink platform.

Key-Words: - Three-Input Integrated DC-DC (TIID) converter, state-space modelling, small-signal analysis, Transfer Function Matrix (TFM), RGA, Contoured Robust Controller Bode Plot (CRCBP), Neutral Point Clamped Inverter, Microgrid

Received: May 14, 2025. Revised: July 9, 2025. Accepted: September 14, 2025. Published: May 13, 2026.

1 Introduction

The switched mode DC-DC converters are the building blocks in many power electronic system applications, namely locomotives and all renewable energy sourced systems like HEVs and HEMs, [1], [2]. The switched-mode DC-DC converters can be single-sourced or multi-sourced. In comparison with single-sourced converters, the Multi-Input Converters (MIC) have been proven to be more flexible, efficient, reliable, and economical, [3]. The MICs can be implemented in many ways (i) MIC converters can be designed by connecting several converters in parallel, [4], [5], [6]. In such MICs, all DC sources cannot participate in each operating mode in a switching cycle when switches operate in a complementary fashion. (ii) The MIC can be designed by use of integrated converters, [7]. (iii) The MIC can be designed such that each source acts independently or in an integrated fashion. The advantages of these integrated MICs are (i) they reduce the number of components to be used, (ii) all the sources are participating in the transfer of power to the load either simultaneously or individually, and (iii) load sharing is possible even if one of the sources fails. All these features make the MICs more reliable, economical, and suitable for applications like the renewable system applications and HEVs, [8]. These advantages led to the proposal of the Three-Input Integrated Bi-directional DC-DC (TIIBD) converter. The TIIBD converter has a smaller number of components compared to conventional three converter-based systems, even other similar converters reported in the literature.

A bidirectional MIC is proposed in [9] using a dc-link and a magnetic coupling. Here, six power switches are required for a single topology. The sources and the load are isolated galvanically. In [10], a three-level DC/DC converter is explained. A novel bidirectional non-isolated MIC topology is suggested in [11]. Unlike its competitors, the converter only needs one extra active switch for each input because its inductors are connected to a single switch, lowering the number of components. In [12], a MIC for HEVs is suggested, and PI controllers are designed using a Matlab-based PID tuner. The design, advantages, and disadvantages of AC-DC and DC-DC converter topologies for

Fast Charging Stations are evaluated in [13], [14]. A four-port converter in [15], is implemented with fewer components and a PI control scheme, increasing the converter's dependability and economy. Various PI control techniques are used in all of these works. The implementation of a PI controller system based on CRCBP for a TIIBD converter for a grid-connected MG is attempted in this study. Robust control and the traditional loop-shaping methodology are combined in the CRCBP method, [16], [17]. This work makes the following contributions:

(i) A fourth-order TIIBD converter is modelled based on the Three-Input dc-dc converter in [18]. Here, two boost converters are merged with a buck-boost converter. The converter operation and dynamics are represented by a mathematical model. State space analysis, along with the small-signal averaging method, is performed in each mode of operation to obtain the TFM.

(ii) To determine the controller structure, interaction analysis is carried out to determine the converter's input-output pairing.

(iii) Further, a CRCBP-based multi-variable controller is proposed for the TIIBD converter, which is a major contribution of the present work.

(iv) A grid-connected MG with the proposed TIIBD converter, with three types of renewable sources: batteries, FC stacks, and PV panels, is designed and implemented with an NPC inverter for power management. The Simulink/ MATLAB environment is used to develop the controllers for the three inputs and evaluate and verify the converter's steady-state performance under various operating situations, all while handling a 10 KW AC load for microgrid applications.

This paper is arranged as the following sections: Section 2 explains operation of TIIBD converter in different modes and steady-state analysis of the converter for every operating mode, section 3 explains the PI controller design based on CRCBP method for MPPT and Battery control, section 4 explains the implementation of TIIBD converter for grid connected MG system and the controllers used for closed loop operation of the converter for a load of 10KW and grid connection. Validation of the designed converter for different operating conditions is given in Section 5, and finally, Section 6 gives the conclusion.

2 Modeling of TIIBD Converter

The proposed TIIBD has 2 unidirectional switches S_1, and S_2 for two inputs PV, FC and 2 bidirectional S_3 and S_4 for charging and discharging of, battery as shown in Figure 1 and Figure 2. These four switches are independently controlled by four duty ratio control signals d_1, d_2 d_3 d_4 which facilitates power flow from three different sources to the load either individually or simultaneously. Thus, $d_3 > d_2 > d_1$ it is chosen to know the converter operation in charging and discharging modes clearly. To understand the TIIBD converter dynamics, a mathematical model is developed. State space analysis is performed in each mode of operation.

The TIIBD converter operates in Continuous Conduction Mode (CCM), and the leading edge ON time synchronized switching sequence is used to interpret the integrated converter operation $d_3 > d_2 > d_1$, which d_3 is complementary to d_4 that shown in Figure 3 using PWM gating signals.

There are four modes of operation for the converter in this switching method. To understand the converter operation and modelling, all the sources, PV, FC, and battery, are all providing the load.

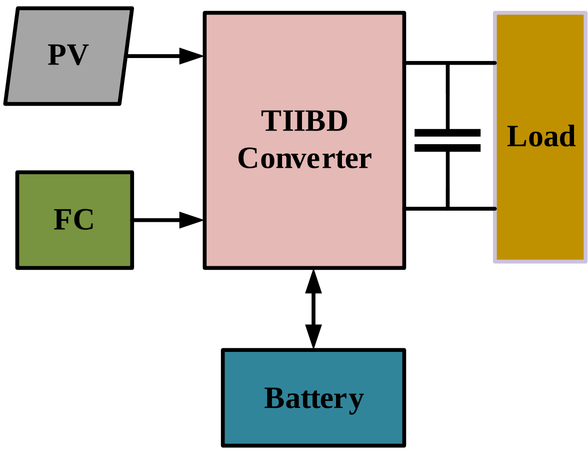

Fig. 1: Block diagram of the TIIBD converter.
Source: created by authors

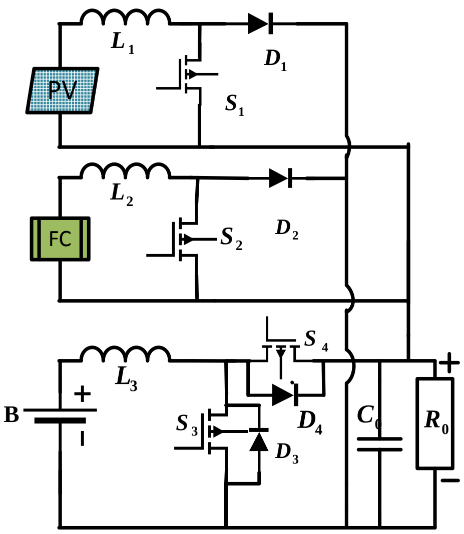

Fig. 2: TIIBD converter with three inputs and a load
Source: created by authors

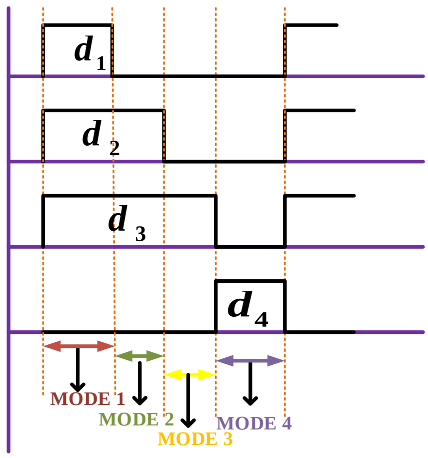

Fig. 3: PWM Gating diagram
Source: created by authors

2.1 Three Sources Supplying the Load

Equations (1) and (2), where i=1,2,3,4 for modes 1, 2, 3, and 4, respectively, provide a set of state equations that readily characterize the dynamics of the power stage in each mode of operation. As a result, we obtain four state equations for each of the four modes.

$$\dot{x} = A_i x + B_i u \text{ , } y = E_{0i} x + F_{0i} u \tag{1}$$

$$y = \begin{bmatrix} v_0 \\ i_{g1} \\ i_{g2} \end{bmatrix} E_{0i} = \begin{bmatrix} E_1 \\ P_{1i} \\ P_{2i} \end{bmatrix} F_{01} = \begin{bmatrix} F_1 \\ F_{1i} \\ F_{2i} \end{bmatrix} \tag{2}$$

The detailed modelling and derivation of TFM for the TIID converter is given in, [19]. The same can be applied to the proposed TIIBD converter.

The output voltage V_{dc} in case(i) depends on source voltages V_{PV}, V_{FC}, V_B and duty ratio control signals d_1, d_2 and d_3 of the integrated converter, it is described using the voltage gain or the voltage conversion ratio as given in (3).

$$V_{dc} = \frac{V_{PV}}{(1-d_1)} = \frac{V_{FC}}{(1-d_2)} = \frac{V_B}{(1-d_3)} \tag{3}$$

3 CRCBP-Based Decentralized Controller for TIIBD Converter

The schematic control diagram of the TIIBD converter is shown in Figure 4. The renewable sources, PV, FC, and battery are controlled by using MPPT techniques along with a PI controller, as shown in Figure 5, Figure 6 and Figure 7. To obtain maximum power from PV and FC, P&O MPPT, along with CRCBP-PI controller, is used as shown in Figure 5 and Figure 6, respectively. The charging and discharging of the battery output is controlled by using SOC control that regulates battery power not to exceed rated power, as shown in Figure. 7.

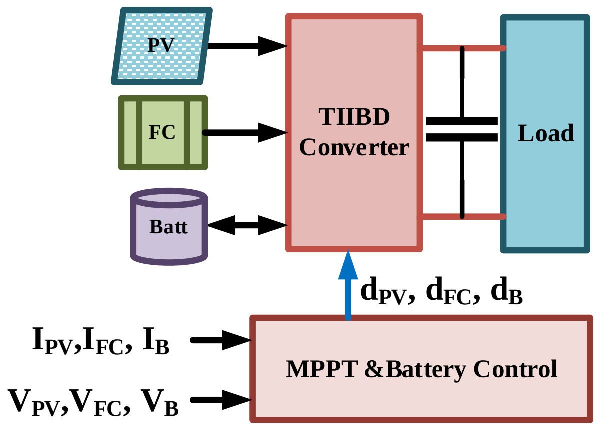

Fig. 4: Control of PV, FC, Battery-sourced TIIBD converter
Source: created by authors

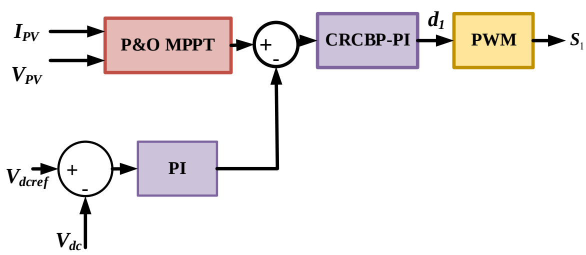

Fig. 5: MPPT control of PV
Source: created by authors

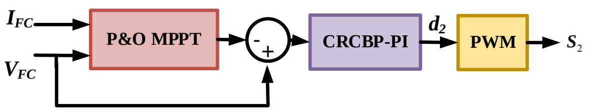

Fig. 6: MPPT control of FC
Source: created by authors

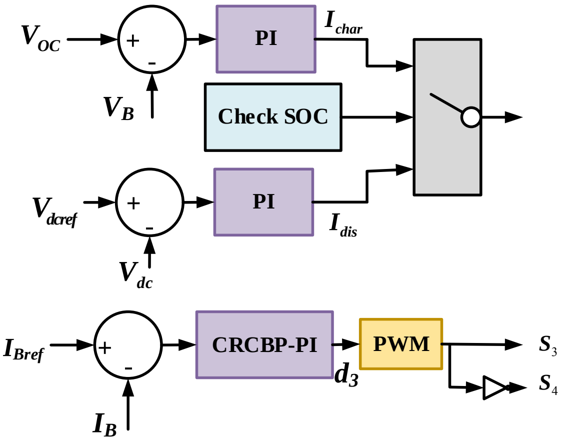

Fig. 7: Battery control using SOC
Source: created by authors

These three PI controllers to control the TIIBD converter are iteratively designed by the CRCBP method. The CRCBP method performs better than the others as described in [17]. In this procedure, the stability and performance are defined with a Robust Performance Metric (RPM) based on the maximum singular value ($\bar{\sigma}$) of WFM as given in (4). In this method, the sufficient condition for a closed-loop converter system to be robust is that the RPM $\Gamma(\omega)<1\ \forall\omega$.

$$\Gamma(\omega)=\bar{\sigma}(W(s))=\bar{\sigma}\left(\left|\begin{bmatrix} W_1S \\ W_2KS \\ W_3T \end{bmatrix}\right|\right) \quad (4)$$

where weight functions W_1 W_2 W_3 represent the sensitivities of the system, respectively. The contours of RPM are drawn on the Bode charts of the controller. The controller is adjusted till its frequency response does not cross the contours of the RPM. In each iteration, the Bode plots of the controller are observed so as not to intersect with forbidden regions of RPM, i.e., $\Gamma(\omega)\geq 1$. If the intersections are found, then the controller is not robust, so the iterations are repeated till a robust controller is obtained.

Before designing the controller, its structure has to be known by the Interaction Measures (IMs). The TFM of the TIIBD converter for the parameters shown in Table 2 is given in (5), which is obtained same way as described in [20].

$$G_{11}=\frac{-35.42s^4-3.542*10^6s^3-3.98*10^7s^2+8.337*10^8s+5.153*10^8}{s^4+126s^3+6.569*10^2s^2+7.201*10^5s+4.134*10^5}$$
$$G_{12}=\frac{2.243*10^4s^3+4.858*10^7s^2+1.883*10^9s+3.328*10^9}{s^4+126s^3+6.569*10^2s^2+7.201*10^5s+4.134*10^5}$$
$$G_{13}=\frac{2.637*10^8s^2-3.203*10^9s-1.845*10^8}{s^4+126s^3+6.569*10^2s^2+7.201*10^5s+4.134*10^5}$$
$$G_{21}=\frac{-2.763s^4+5.42*10^6s^3+1.243*10^8s^2+5.091*10^8s+2.771*10^8}{s^4+126s^3+6.569*10^2s^2+7.201*10^5s+4.134*10^5}$$
$$G_{22}=\frac{-1734s^3-7.036*10^7s^2-1.614*10^9s-6.098*10^9}{s^4+126s^3+6.569*10^2s^2+7.201*10^5s+4.134*10^5}$$
$$G_{23}=\frac{-4.933*10^4s^3-4.094*10^8s^2-3.244*10^9s-6.166*10^9}{s^4+126s^3+6.569*10^2s^2+7.201*10^5s+4.134*10^5}$$
$$G_{31}=\frac{54.26s^4-2.665*10^5s^3+2.597*10^8s^2+2.154*10^8s+3.04*10^7}{s^4+126s^3+6.569*10^2s^2+7.201*10^5s+4.134*10^5}$$
$$G_{32}=\frac{88.27s^3+3.498*10^6s^2-3.319*10^9s-1.385*10^8}{s^4+126s^3+6.569*10^2s^2+7.201*10^5s+4.134*10^5}$$
$$G_{33}=\frac{6.406*10^5s^3+8.725*10^7s^2+2.108*10^{10}s+1.437*10^{10}}{s^4+126s^3+6.569*10^2s^2+7.201*10^5s+4.134*10^5} \quad (5)$$

For this TFM G, RGA is calculated to find the controller structure and it is given in (6), indicating a diagonal/ decentralised controller structure as given in [20]. Thus, to design G_{c1} for G_{11}, the Weight Function Matrix (WFM) is to be constructed first, [21]. W_1 And W_3 are selected as given in (7).

$$RGA(G(s))=\begin{bmatrix} 0.7663 & 0.2226 & 0.0111 \\ 0.2332 & 0.7595 & 0.0073 \\ 0.0005 & 0.0179 & 0.9817 \end{bmatrix} \quad (6)$$

$$W_1=\frac{s+150}{1.5s+300}, W_2=0, W_3=\frac{s+5000}{0.01s+1*10^4} \quad (7)$$

The controller's effort is not limited to $W_2=0$. The detailed iterative procedure for designing the CRCBP controller is given in [17].

Primarily, G_{c1} it is taken as a Proportional Controller ($K_P=1$). Figure 8 displays the CRCB charts for the closed-loop system. The area G_{c1} where the forbidden region intersects is indicated by the red part ($\Gamma(\omega)\geq 1$), implying that the designed controller is not robust.

Figure 10 shows the Bode Magnitude Frequency Response (BMFR) of $1/W_1$, S_1 and $1/W_3$, T_1 and indicates that $1/W_3$ is below T_1 in the high frequency region. Thus, the closed-loop complementary sensitivity function violates the constraint in the high frequency region, indicating that the system is exhibiting poor disturbance rejection characteristics, which caused the interaction with the forbidden region in the high frequency region, as shown in Figure 9. So, the controller needs to have integral action to compensate for this.

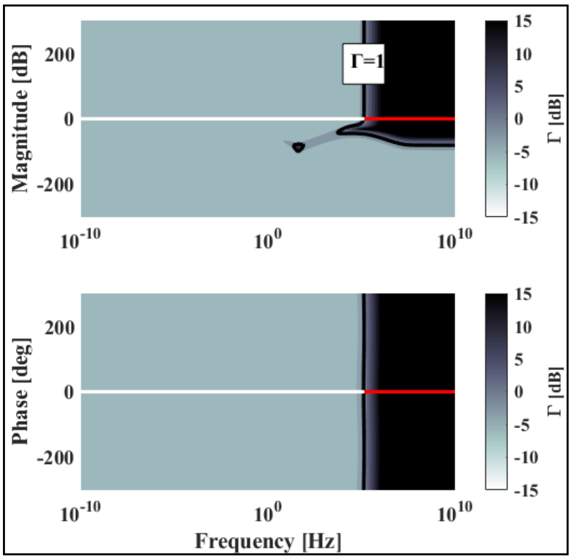

Fig. 8: CRCBP of G_{c1} and G_{11} in iteration 1
Source: created by authors

G_{c1} It is taken solely as an Integral Controller ($K_I = 0.0005$). The CRCB plots and BMFR are shown in Figure 11 and Figure 12, respectively, and show that there are no interactions with the forbidden region, implying the robustness of the controller. Figure 12 shows that $1/W_1$ and $1/W_3$ satisfy the upper bounds of S_1 and T_1.

Similarly, G_{c2} and G_{c3} are designed and given below in (8) and (9).

$$G_{c2} = \frac{0.004s^2 + 0.03s + 2.9171}{s^2 + 1000s} \quad (8)$$

$$G_{c3} = \frac{6.94*10^{-5}s + 0.00521}{s} \quad (9)$$

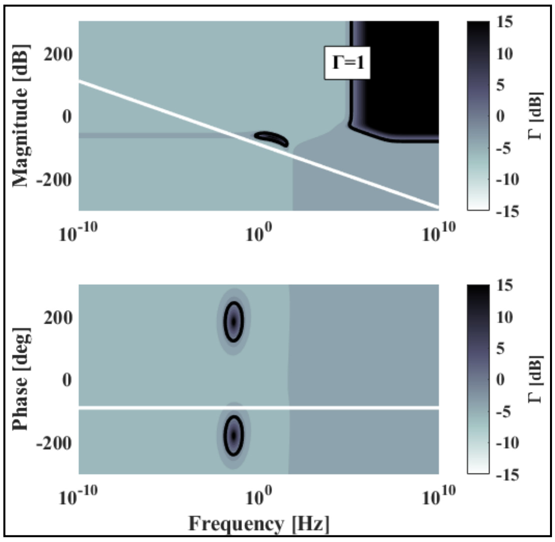

Fig. 9: CRCBP of G_{c1} and G_{11} in iteration 2
Source: created by authors

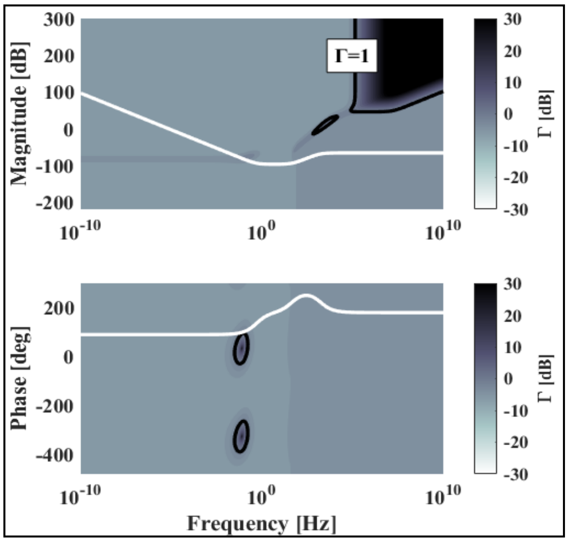

Fig. 10: CRCBP of G_{c2} and G_{22}
Source: created by authors

The CRCB plots are shown in Figure 10 and Figure 11, respectively. The BMFR of their weight functions and sensitivities are given in Figure 12 and

Figure 13, respectively. Corresponding step responses of the 3 Closed-Loop Systems (CLS) are given in Figure 14. The obtained CRCBP controller performance is compared with the SISO tuned PID controller [23] as shown in Figure 15. The time domain parameters of the two controllers for the system G_{11} are compared and shown in Table 1. The CRCBP controller outperformed the PI controller in terms of performance.

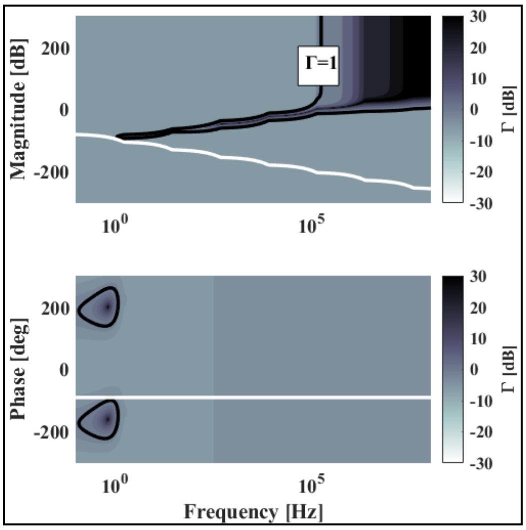

Fig. 11: CRCBP of G_{c3} and G_{33}

Source: created by authors

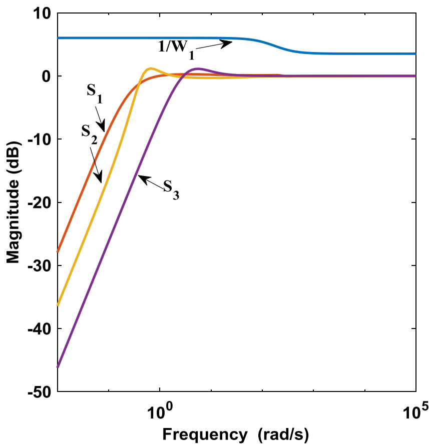

Fig. 12: BMFR of $1/W_1$ and sensitivities

Source: created by authors

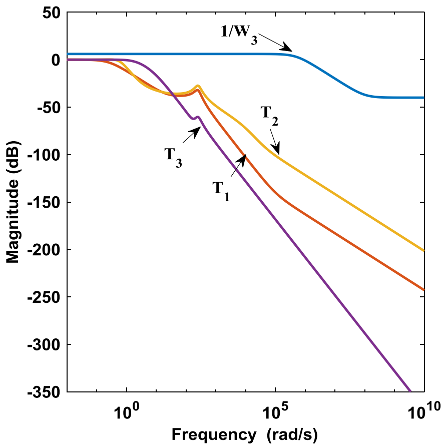

Fig. 13: BMFR of $1/W_3$ and complementary sensitivities

Source: created by authors

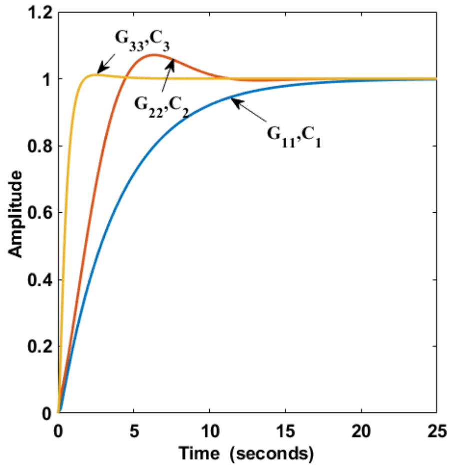

Fig. 14: Step responses of three CLSs

Source: created by authors

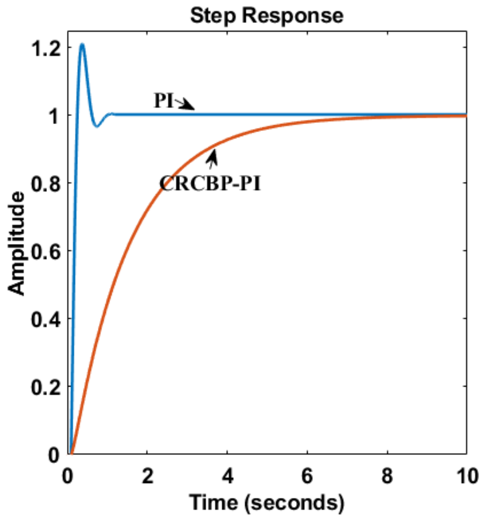

Fig. 15: Comparison of PI and CRCBP controller performance of G_{11} the system

Source: created by authors

Table 1. Comparison of PI and CRCBP controller performance of G_{11} the system

Controller for G_{11}	PI	CRCBP
Rise Time	0.1196	3.2159
Transient Time	0.7649	5.8971
Settling Time	0.8495	5.9145
Overshoot	21.1197	0
Undershoot	57.4093	1.1382
Peak	1.2112	0.9998
Peak Time	0.3720	12.8303

Source: created by authors

4 Implementation of TIIBD for Grid-Connected MG

Neutral Point Clamped (NPC) Inverter with three levels is used to connect the TIIBD converter, three inputs (PV, FC, and battery), and the grid (Figure 19). In comparison to conventional two-level inverters, neutral point is clamped to DC bus voltage midpoint via diodes, resulting in decreased harmonic distortion and increased efficiency, [24], [25]. The output from the inverter is filtered out with an LCL filter and is connected to the load and to the Circuit Breaker (CB), then to the utility grid via a transformer. The CB switch is switched based on the availability of power from sources. Whenever the Input Power is sufficient to supply the load, the CB device is in the OFF state. If the P_{in} is either a surplus or a deficiency, then CB it is switched on to either supply to the grid or to take from the grid. The algorithm to connect and disconnect the MG to the grid is given below.

Algorithm for Grid-connected TIIBD Converter
Get $V_{dc}, V_{PV}, V_{FC}, V_B, P_{PV}, P_{FC}, P_B, P_L, CB$ Calculate $P_{in} = P_{pv} + P_{fc} + P_b$ if $P_{in} = P_L$ $CB = 1$ else $CB = 0$ end

4.1 Control of NPC Inverter with Dq Control

The output of the NPC-VSI must be fully in phase and frequency synchronization with the grid since the three-level NPC Inverter is connected to both the load and the grid. Thus, the modulating signal, which controls the inverter, is in charge of synchronizing the output voltage of the inverter. The current control loop's output is the modulating signal for the inverter. In order to convert the real grid quantities into dq quantities, the current is managed in a synchronous dq rotating frame. Park transformation is then used to rotate the reference frame synchronously with the grid voltage vector, converting the grid quantities into DC values. The inverter current is then controlled by the PI controller. Through independent control of the current in the d and q axes, the active and reactive power may be managed. In addition, because it is intended for the rotating frame to move in unison with the grid voltage's frequency and phase angle, the grid angle is necessary to perform the Park transformation, which is extracted using the Phase Locked Loop (PLL) managed by d-q control, [26]. Figure 16 depicts the control structure.

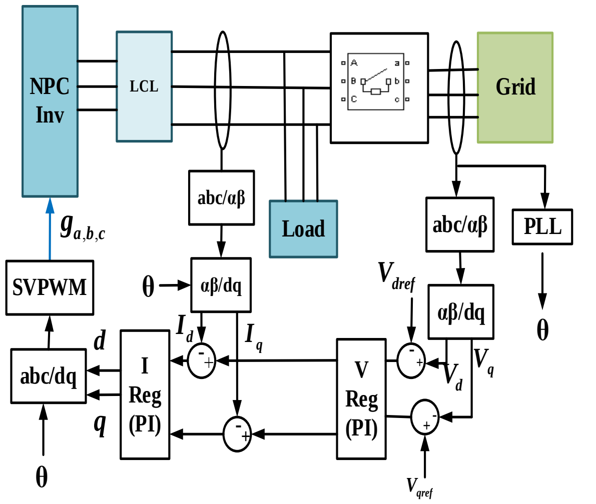

Fig. 16: Control of NPC Inverter with dq control
Source: created by authors

4.2 Design Specifications for HEMS Application

A Microgrid with a load of 10KW connected to a 3-Ø, 415V Utility Grid and a 700V DC link voltage is selected in order to verify the TIIBD converter operation for the MG system. In order to distribute the load demand, the sources are set up so that PV provides 70% of the load, FC delivers 30% of the load, and the Battery can offer 2% of the load if the other two sources are unavailable. Table 2 provides the parameters needed for the load and source specifications mentioned above.

5 Results

The grid-connected MG system with TIIBD converter is implemented in MATLAB environment for the specifications given in Table 1 under nominal operating conditions, and the closed-loop performance of the system is studied in different operating conditions.

Table 2. Specifications to validate the TIIBD converter

Name	Specification/value
PV panel	Sun Earth Solar-160W, N_s=8, N_p=6
Battery	12Ah,180V
Fuel Cell	PEMFC 6KW,48V
Inductors	$L_1 = 0.0011H$, $L_2 = 0.0313H$, $L_3 = 0.046H$
DC Link Voltage	$V_{dc} = 700V$
DC link Capacitors	$C_o = 1200\mu F$
LCL Filter	$L_{1f} = L_{2f} = 0.005H$,

Name	Specification/value
	$C_f = 500\mu F$
Switching frequency f_s	10KHz
Load (P_L)	10KW,415V
Transformer	415V/11KV,50 Hz
Utility Grid Voltage	11KV

Source: created by authors

5.1 Case (i) Nominal Operating Conditions

The DC output voltage (V_{dc}) of the TIIBD converter of 700V, along with the input voltages of PV, FC, and Battery, is shown in Figure 17.

This V_{dc} is fed to a 3-level NPC Inverter, and the inverter output voltage(V_{inv}) is shown in Figure 18. The filtered output voltage is shown in Figure 19. The three input powers are shown in Figure 20. The P_{in} and P_L of the MG system are shown in Figure 21, and the THD of the generated AC voltage (V_{AC}) is shown in Figure 22. The THD is found to be 3.16% which is in the permissible limits.

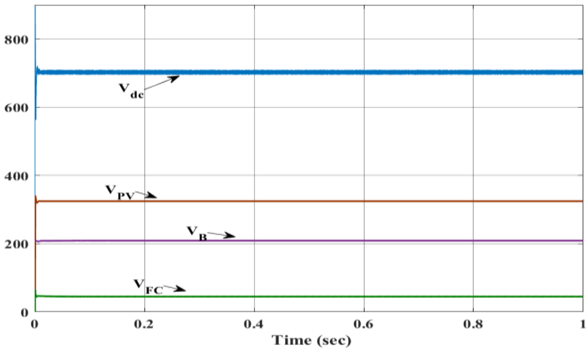

Fig. 17: Input and output voltages of TIIBD Converter
Source: created by authors

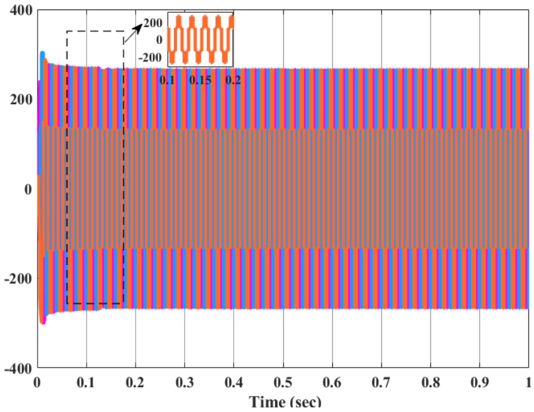

Fig. 18: Output voltage of NPC Inverter
Source: created by authors

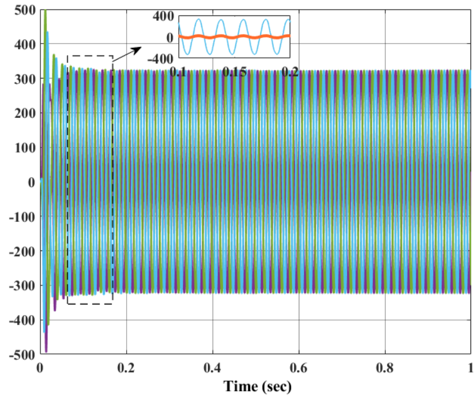

Fig. 19: 3-ph output Voltages and currents after filtering
Source: created by authors

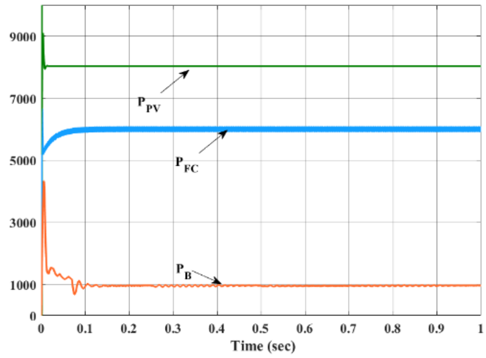

Figure. 20. Input Powers of PV, FC, and Battery
Source: created by authors

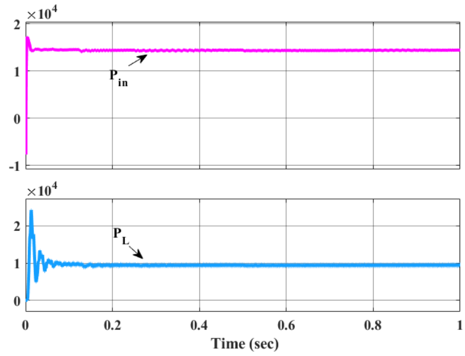

Fig. 21: P_{in} and P_L of the MG system
Source: created by authors

5.2 Case (ii) Under Load Variation

The load at the AC Bus is varied from 10KW to 12KW at t=0.1sec and from 12 KW to 10 KW at t=0.2 sec. The output phase voltages are given in Figure 23. It can be seen from this Figure that the output voltage is regulated with the dq controller.

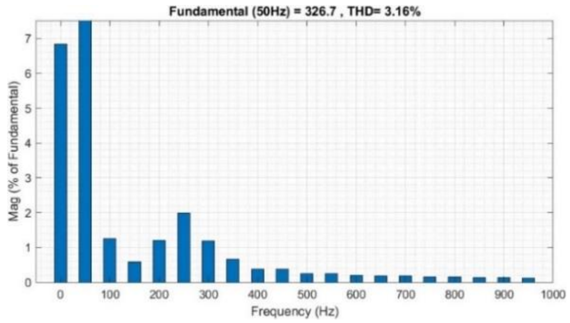

Fig. 22: THD of the output phase voltage after filtering
Source: created by authors

5.3 Case (iii) Under Irradiance Change

The solar irradiance is varied, and the controller can track the corresponding P_{max} as shown in Figure 24. The corresponding input voltages and the regulated V_{dc} output are shown in Figure 25.

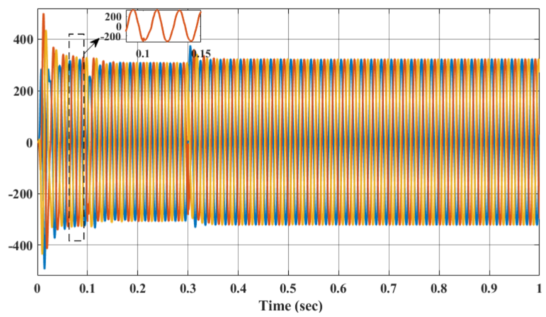

Fig. 23: The regulated 3-phase output voltage with load variations
Source: created by authors

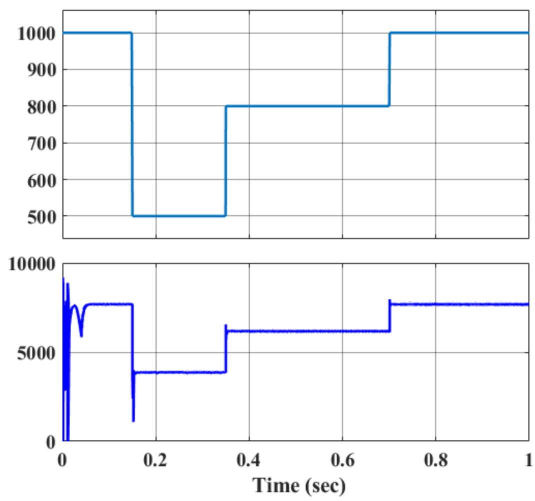

Fig. 24: The irradiance variations and P_{max} with time
Source: created by authors

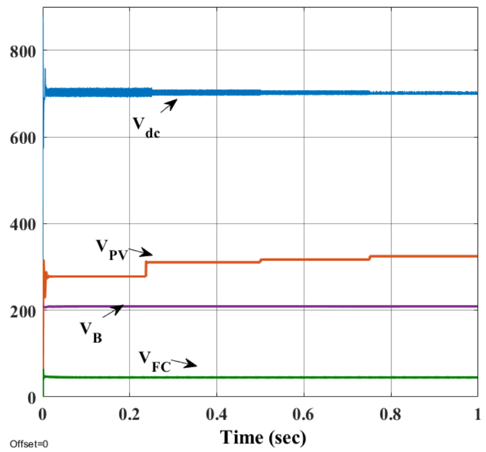

Fig. 25: The regulated output voltage with Irradiation variations
Source: created by authors

6 Conclusion

For grid-connected MG applications, the TIIBD converter is constructed using three renewable sources: PV, FC, and battery. Small-signal analysis is used to model the converter and obtain TFM. PI controllers for the MPPT control of PV, FC, and battery control of the converter are designed using the CRCBP approach. Between the grid and the TIIBD converter is a three-level NPC inverter, and the inverter is controlled using a PLL based on the dq technique. The microgrid's connection and disconnection from the grid are managed by an algorithm that relies on power surplus. In a MATLAB environment, the performance of the TIIBD converter is confirmed under various operating circumstances.

The Future scope of this research work is (i) to perform a comparative analysis of the designed controller with H_∞ controller, Fuzzy and ANN methods, (ii) to perform stability analysis, component tolerances, switching losses and thermal considerations, (iii) to design a small-scale hardware prototype to validate the controller performance for MG system with real-time experimental results and (iv) to combine the CRCBP controller with other metaheuristic methods like Genetic Algorithm and Particle Swarm Optimization and implement the MG system.

References:

[1] X. L. Li, Z. Dong, C. K. Tse, and D. D. -C. Lu, "Single-Inductor Multi-Input Multi-Output DC–DC Converter with High Flexibility and Simple Control," in *IEEE*

Transactions on Power Electronics, vol. 35, no. 12, pp. 13104-13114, Dec. 2020. 10.1109/ISCAS45731.2020.9180788

[2] A. Gupta, R. Ayyanar, and S. Chakraborty, "Novel Electric Vehicle Traction Architecture With 48 V Battery and Multi-Input, High Conversion Ratio Converter for High and Variable DC-Link Voltage," in *IEEE Open Journal of Vehicular Technology*, vol. 2, pp. 448-470, 2021. https://doi.org/10.1109/OJVT.2021.3132281

[3] B. R. Ravada, N. R. Tummuru, and B. N. L. Ande, "Photovoltaic-Wind and Hybrid Energy Storage Integrated Multi-Source Converter Configuration for DC Microgrid Applications," in *IEEE Transactions on Sustainable Energy*, vol. 12, no. 1, pp. 83-91, Jan. 2021. https://doi.org/10.1109/TSTE.2020.2983985

[4] E. Amiri, R. R. Khorasani, E. Adib, and A. Khoshkbar-Sadigh, "Multi-Input High Step-Up DC–DC Converter with Independent Control of Voltage and Power for Hybrid Renewable Energy Systems," in *IEEE Transactions on Industrial Electronics*, vol. 68, no. 12, pp. 12079-12087, Dec. 2021, https://doi.org/10.1109/TIE.2020.3047038.

[5] Narayanaswamy, J.; Mandava, S. Non-Isolated Multiport Converter for Renewable Energy Sources: A Comprehensive Review. *Energies* **2023**, *16*, 1834. https://doi.org/10.3390/en16041834

[6] Soldado-Guamán, J.; Herrera-Perez, V.; Pacheco-Cunduri, M.; Paredes-Camacho, A.; Delgado-Prieto, M.; Hernandez-Ambato, J. Multiple Input-Single Output DC-DC Converters Assessment for Low Power Renewable Sources Integration. *Energies* **2023**, *16*, 1652. https://doi.org/10.3390/en16041652

[7] Yuan-Chuan Liu and Yaow-Ming Chen, "A Systematic Approach to Synthesizing Multi-Input DC–DC Converters," *IEEE Transactions on Power Electronics*, vol. 24, no. 1, January 2009, pp. 116-127. 10.1109/TPEL.2008.2009170

[8] Akar, Y. Tavlasoglu, E. Ugur, B. Vural, and I. Aksoy, "A Bidirectional Nonisolated Multi-Input DC–DC Converter for Hybrid Energy Storage Systems in Electric Vehicles," in *IEEE Transactions on Vehicular Technology*, vol. 65, no. 10, pp. 7944-7955, Oct. 2016, https://doi.org/10.1109/TVT.2015.2500683.

[9] H. Tao, A. Kotsopoulos, J. L. Duarte, and M. A. M. Hendrix, "Multi-input bidirectional DC-DC converter combining DC-link and magnetic-coupling for fuel cell systems," *Fortieth IAS Annual Meeting. Conference Record of the 2005 Industry Applications Conference*, 2005., Hong Kong, China, 2005, pp. 2021-2028 Vol. 3 https://doi.org/10.1109/IAS.2005.1518725.

[10] S. Dusmez, A. Hasanzadeh, and A. Khaligh, "Comparative Analysis of Bidirectional Three-Level DC–DC Converter for Automotive Applications," in *IEEE Transactions on Industrial Electronics*, vol. 62, no. 5, pp. 3305-3315, May 2015, https://doi.org/10.1109/TIE.2014.2336605.

[11] Akar, Y. Tavlasoglu, E. Ugur, B. Vural, and I. Aksoy, "A Bidirectional Nonisolated Multi-Input DC–DC Converter for Hybrid Energy Storage Systems in Electric Vehicles," in *IEEE Transactions on Vehicular Technology*, vol. 65, no. 10, pp. 7944-7955, Oct. 2016, https://doi.org/10.1109/TVT.2015.2500683.

[12] R. R. Ahrabi, H. Ardi, M. Elmi, and A. Ajami, "A Novel Step-Up Multi-Input DC–DC Converter for Hybrid Electric Vehicles Application," in *IEEE Transactions on Power Electronics*, vol. 32, no. 5, pp. 3549-3561, May 2017, https://doi.org/10.1109/TPEL.2016.2585044

[13] F. Kardan, R. Alizadeh, and M. R. Banaei, "A New Three-Input DC/DC Converter for Hybrid PV/FC/Battery Applications," in *IEEE Journal of Emerging and Selected Topics in Power Electronics*, vol. 5, no. 4, pp. 1771-1778, Dec. 2017, https://doi.org/10.1109/JESTPE.2017.2731816

[14] Chakraborty, S.; Vu, H.-N.; Hasan, M.M.; Tran, D.-D.; Baghdadi, M.E.; Hegazy, O. DC-DC Converter Topologies for Electric Vehicles, Plug-in Hybrid Electric Vehicles and Fast Charging Stations: State of the Art and Future Trends. *Energies* 2019, 12, 1569. https://doi.org/10.3390/en12081569

[15] Kothandan Suresh, Harini Sampath, Nallaperumal Chellammal, Satish R. Jondhale, and Chokkalingam Bharatiraja, “Modular Multi-Input Bidirectional DC to DC Converter for Multi-Source Hybrid Electric Vehicle Applications”, *Journal of Applied Science and Engineering*, 2021, Vol. 25, No. 3, Page 389-399.

https://doi.org/10.6180/jase.202206_25(3).0004

[16] M. Veerachary and P. Shaw, "Controller Design and Analysis for Fifth-Order Boost Converter," in *IEEE Transactions on Industry Applications*, vol. 54, no. 5, pp. 4894-4907, Sept.-Oct. 2018, https://doi.org/10.1109/TIA.2018.2843758

[17] J. D. Taylor and W. Messner, "Controller Design for Nonlinear Multi-Input/Multi-Output Systems Using The Contoured Robust Controller Bode Plot" *International Journal Of Robust And Nonlinear Control*, vol. 24, no. 18, pp. 3196–3213, 2013, https://doi.org/10.1002/rnc.3049.

[18] M. Manogna, A. B. Amarendra Reddy, and K. Padma, "Modeling of a Three-Input Fourth-Order Integrated DC-DC Converter," in *Proceedings - 2022 International Conference on Smart and Sustainable Technologies in Energy and Power Sectors, SSTEPS 2022*, Institute of Electrical and Electronics Engineers Inc., 2022, pp. 83–88. https://doi.org/10.1109/SSTEPS57475.2022.00032

[19] Y. -C. Liu and Y. -M. Chen, "A Systematic Approach to Synthesizing Multi-Input DC–DC Converters," in *IEEE Transactions on Power Electronics*, vol. 24, no. 1, pp. 116-127, Jan. 2009, https://doi.org/10.1109/TPEL.2008.2009170

[20] M. Manogna, B. A. Reddy, and K. Padma, "Interaction measures in a three-input integrated DC-DC converter," *Engineering Research Express*, vol. 5, no. 1, Mar. 2023, https://doi.org/10.1088/2631-8695/acc0dc.

[21] K. and J. C. Doyle. Zhou, *Essentials of Robust Control. Upper Saddle River: Prentice-Hall, 1999.ISBN 978-0135258330.*

[22] T. H. K. J Åström, *Advanced PID control*. Instrumentation, Systems, and Automation Society Research Triangle Park, NC, 2006. *ISBN 978-1556179421.*

[23] Akash S. Pabbewar, M. Kowsalya," Three Level Neutral Point Clamped Inverter Using Space Vector Modulation with Proportional Resonant Controller," *Energy Procedia*, Volume 103,2016, Pages 286-291, ISSN 1876-6102, https://doi.org/10.1016/j.egypro.2016.11.287

[24] H. Dehghani Tafti, A. I. Maswood, A. Ukil, O. H. P. Gabriel, and L. Ziyou, "NPC photovoltaic grid-connected inverter using proportional-resonant controller." *2014 IEEE PES Asia-Pacific Power and Energy Engineering Conference (APPEEC)*. IEEE, 2014. https://doi.org/10.1109/APPEEC.2014.7066201

[25] A. Ravi, P.S. Manoharan, J. Vijay Anand, "Modelling and simulation of three-phase multilevel inverter for grid-connected photovoltaic systems", *Solar Energy*, Volume 85, Issue 11,2011, Pages 2811-2818, ISSN 0038-092X, https://doi.org/10.1016/j.solener.2011.08.020

[26] Natarajan, Prabaharan, & Kaliannan, Palanisamy. (2017). A comprehensive review of reduced switch multilevel inverter topologies, modulation, techniques, and applications. Renewable and Sustainable Energy Reviews. 76C. 1248-1282. https://doi.org/10.1016/j.rser.2017.03.121.

Contribution of Individual Authors to the Creation of a Scientific Article (Ghostwriting Policy)

The authors equally contributed to the present research, at all stages from the formulation of the problem to the final findings and solution.

Sources of Funding for Research Presented in a Scientific Article or the Scientific Article Itself

No funding was received for conducting this study.

Conflict of Interest

The authors have no conflicts of interest to declare.